Journal of MATERIALS RESEARCH

MRS Fellows Focus Review
DOI:10.1557/s43578-023-01229-w

# Defects at nanoscale semiconductor interfaces: Challenges and opportunities

Leonard J. Brillson[1,a]

[1] Department of Electrical & Computer Engineering and Department of Physics, The Ohio State University, Columbus, OH 43210, USA
[a] Address all correspondence to this author. e-mail: brillson.1@osu.edu

Received: 6 October 2023; accepted: 8 November 2023; published online: 29 November 2023

**The past 75 years has been an exciting and dynamic time for solid-state electronic materials with advanced micro- and optoelectronic properties but point defects at semiconductor–metal interfaces that limit their operation have been a challenge to understand and control. These defects depend strongly on chemical structure at the intimate interface, and techniques have now developed to learn how their presence at nanoscale dimensions impact electronic structure at the macroscale. A combination of optical, electronic, and microscopic techniques can now enable new directions for defect research of metal–semiconductor interfaces at the nano/atomic scale. These nanoscale and atomic scale techniques can meet the experimental challenges inherent at this scale and create opportunities for new defect research of electronic material interfaces at a deeper level.**

## Introduction—impact of defects on semiconductor interfaces

The nature of semiconductor interfaces with other materials and the impact of their defects on electronic properties has been of major research importance for over 75 years. In particular, the materials research of semiconductor interfaces with metals, insulators and other semiconductors has a rich history in which the Materials Research Society has played a major role. Since its inception fifty years ago, MRS has helped lead the understanding of semiconductor interfaces, driven first by industry's need to make useful, predictable, and controllable contacts to metals and insulators in computer chips. Even before the invention of the transistor, the physical nature of the semiconductor–metal interface, the mechanisms controlling its charge rectification, and its applications have been of wide interest, generating hundreds of thousands of publications to date. Much early work centered on the materials science of the metal–silicon and silicon dioxide interfaces, particularly the interdiffusion and chemical reactions that could take place at their interfaces [1]. That branch of research addressed the materials interactions that determined the electrical resistivity and thermodynamic stability of those semiconductor interfaces. Nevertheless, technologists were also aware of the presence of electronic traps in and at the interfaces of the dielectrics needed for gate biasing of transistors—a realization described by John Bardeen to explain the reduced effect of transistor biasing [2]. Reflecting the rapidly expanding interest in semiconductor interfaces, MRS provided a platform for sharing research on defects in semiconductors. In the first MRS Proceedings issue published in 1980, defects in semiconductors comprised a major symposium with topics ranging across structural and electronic properties, techniques to measure them, and the effects of processing including ion implantation and radiation damage [3]. Indeed, since then, there have been more than 67 published MRS symposia on interfaces including the measurement and electronic impact of defects. By the late 1950's, the drive for higher speed and optoelectronics had expanded research interests in semiconductor interface defects from Si to GaAs and other compound semiconductors. This review will first address how native point defects and impurities depend strongly on interface chemical structure, then how defects at nanoscale semiconductor–metal interfaces impact electronic structure, then how combining optical, electronic, and microscopic techniques provides a new direction for defect research at the nano/atomic scale, and finally the challenges and opportunities for new defect research at electronic material interfaces at a deeper level.

## Defects and interface chemical structure

With the advent of ultrahigh vacuum (UHV) hardware, growth and analytic techniques to explore semiconductor surfaces and interfaces, researchers worldwide began to focus on the fundamental electronic properties of ideal metal–semiconductor interfaces, free from any intervening impurities [4–6]. Using ultraviolet photoemission spectroscopy (UPS) and X-ray photoemission spectroscopy (XPS), researchers worldwide were now able to monitor the Fermi level movements and band bending of semiconductors as metal atoms were added, submonolayer by monolayer, to form rectifying, *i.e.*, Schottky barrier, and ohmic contacts [7–9]. With electron loss spectroscopy (ELS), Auger electron spectroscopy, and electron dispersive X-ray spectroscopy (EDX), it became possible to show how metal atoms can react with semiconductor surfaces to produce new interfacial species,even near room temperature [10, 13]! Furthermore, as shown in Fig. 1(a), these interactions appeared to follow thermodynamics so that metals that could form more stable metal-anion products exhibited a threshold of electronic behavior, *i.e.*, Schottky barrier formation, between reactive vs unreactive metal—semiconductor interfaces.10.

The development of soft x-ray photoemission spectroscopy (SXPS) further expanded the range of interfacial processes due to metal deposition on semiconductors. These included metal indiffusion and semiconductor outdiffusion, materials processes that until then seemed to be limited to high temperature thermal processing. As shown in Fig. 1(b), room temperature semiconductor outdiffusion for metals deposited on compound semiconductors such as InP in particular could be non-stoichiometric with anion outdiffusion sensitive to even single monolayers of reactive vs unreactive species [14, 15]. This unbalanced outdiffusion could result in missing atoms in the outermost semiconductor layers, which could result in charge sites near the metal interface, which in turn could control the Fermi level movement and resultant band bending. In this sense, there was now a "chemical basis" for Schottky barrier formation.

SXPS provided further evidence for the influence of interface material interactions on the metal–semiconductor charge transfer. The charge transfer between semiconductor and metal changes the band bending within the semiconductor and the resultant Schottky barrier height between the semiconductor band edges and the metal Fermi level $E_F$. As a result, $E_F$ relative to the semiconductor band edges changes as layer upon layer of metal deposits on the (clean) semiconductor surface. Figure 2 shows this process for different metals on InP. The final $E_F$ position after 10–20 nm metal thickness signifies the final band bending and $E_C$—$E_F$ Schottky barrier height of the now metallic overlayer. Figure 2 shows these differences in $E_F$ energies and their evolution with metal layer thickness [16]. Each metal exhibits a rapid $E_F$ movement to different bandgap energies with only a few Å deposited metal coverage followed by additional movements to final $E_C$—$E_F$ positions, energies which span nearly half the InP bandgap rather than a narrow range of "pinning" energies. These additional movements vary in both magnitude and direction depending on the specific metal—lattice chemical bonding.

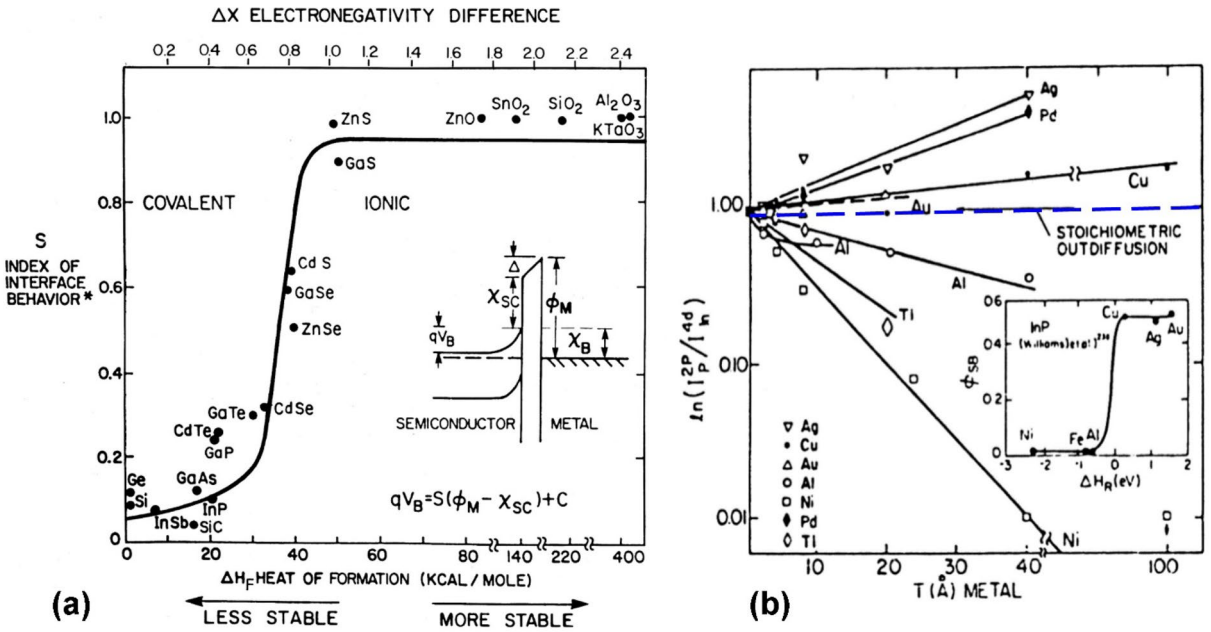


**Figure 1:** (a) Transition in Schottky barrier formation with interface chemical reactivity. [10] (b) Stoichiometry of metal—InP outdiffusion vs reactivity and Schottky barrier height [11, 12].

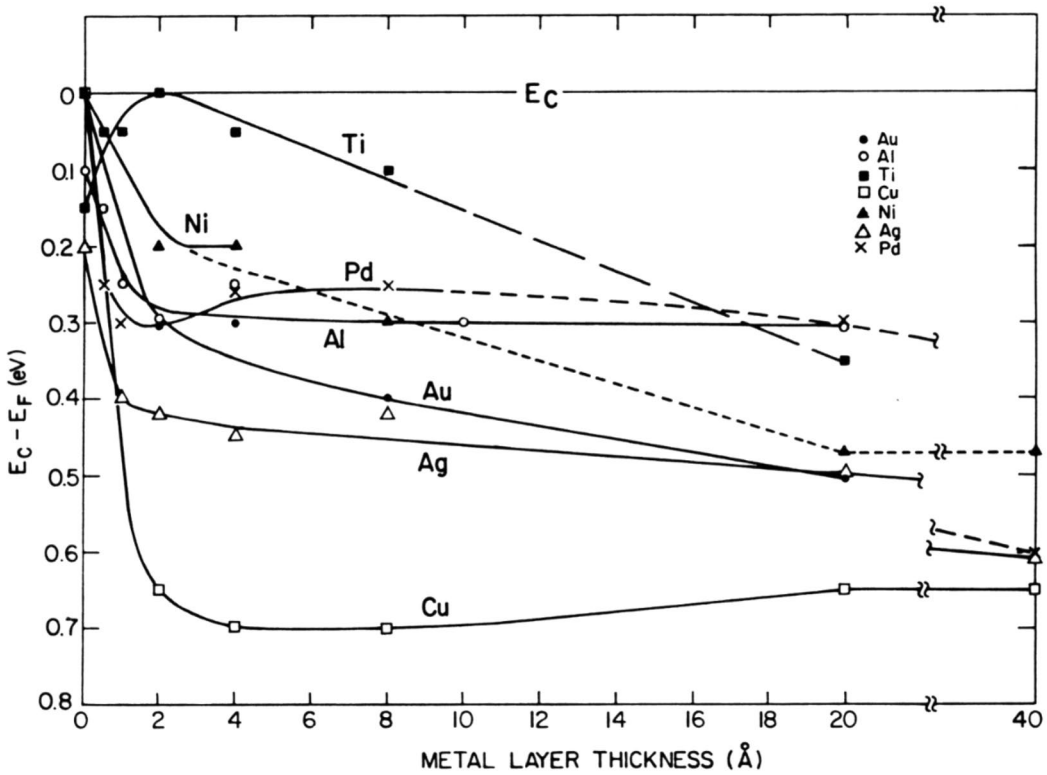


**Figure 2:** $E_F$ movements versus metal overlayer thickness for various metals on UHV-cleaved InP surfaces. Differences in metal–InP interactions are due to different interface material interactions as well as differences in metal electronegativities [16].

Together with defects in the semiconductor bulk [17], these processes provided a picture of semiconductor—metal interfaces which is extrinsic, in contrast to intrinsic models of ideal, unreactive semiconductor–metal interfaces [18–21]. This extrinsic picture could then account for why rectifying metal–semiconductor contacts did not vary systematically with the difference in work function between metal and semiconductor, *i.e.*, Schottky–Mott ideal behavior. Rather, specific materials interactions at the atomic-scale metal–semiconductor interface could account for Fermi level movements which would otherwise be "pinned" in a narrow range due only to surface defects.

## Defects at the nanoscale and interface electronic properties

These metal-specific results showed that electrically active defects could involve more than the outermost semiconductor monolayer. A relatively undeveloped technique provided a way to measure the defects both at and below the metal–semiconductor interface. This depth-resolved cathodoluminescence spectroscopy (DRCLS), extended to UHV environments from early scanning electron microscope studies [22], could probe electronic transitions involving defects within semiconductors, their spatial distribution on a nanometer scale, and their relation to the materials processes described in previous decades. Due to its ability to probe from near-monolayers to microns below the semiconductor surface and even through metal contacts [23], DRCLS provides a range of information about defects at electronic interfaces. These studies included defects induced by strain, dislocations [24, 25], ionizing radiation [26], oxidation [27], heterojunction growth and diffusion [28], surface treatments such as plasma deposition, cleaning, etching and annealing [29], quantum well interface states [30], polytype transformations [31, 32], grain boundary segregation [33], and growth – sensitive processes of next-generation dielectrics and ferroelectrics [34–37].

The DRCLS process shown in Fig. 3 involves an incident electron beam which generates a cascade of secondary electrons whose energies steadily decrease with X-ray generation and plasmon energy loss [38]. Ultimately, these electrons have only enough energy for impact ionization, *i.e.*, incident electron collisions with atomic orbital electrons to eject those electrons, resulting in free electrons and holes within the material's conduction and valence bands, respectively. These free electrons and holes can then recombine via several pathways to emit light, specifically, conduction band-to-valence band transitions and transitions between gap states and those bands. The depth of impact ionization and cathodoluminescence excitation depends on the lattice scattering of the cascading secondary electrons, which in turn depends on both material parameters, *e.g.*, density

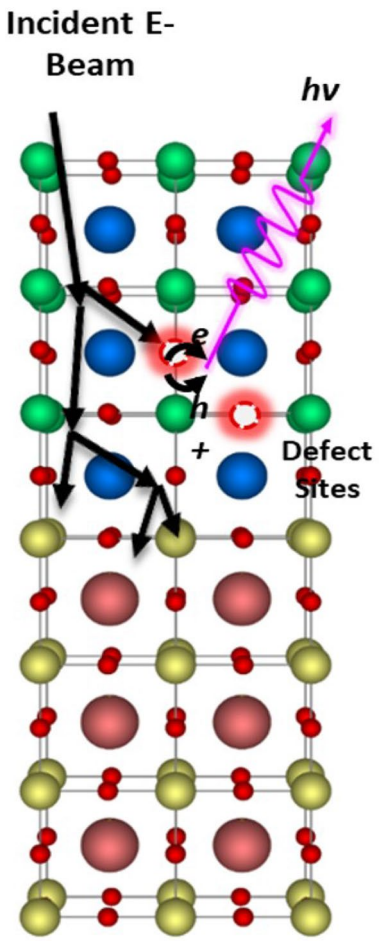


**Figure 3:** DRCLS excitation process consisting of an incident electron that generates a cascade of secondary electrons, producing impact ionization, and the recombination of free holes with electrons which generates optical emission characteristic of lattice defects and the bandgap.

ρ, atomic weight A, atomic number Z, and Avogadro's number $N_A$ and the incident electron beam's energy $E_B$. Monte Carlo simulations statistically determine the depths at which a cascade of electrons generates electron–hole pairs for a selected incident beam energy [39]. For $E_B$ ranging from a few hundred volts to several kilovolts, typical semiconductor excitation depths range from only a few nm to a few hundred nanometers, respectively, depending on the material parameters and film thicknesses through which the incident electron beam traverses.

Figure 4 Left shows DRCL spectra of excitation through 30 nm thick Au vs Ta on ZnO(000–1) surfaces, resulting in excitation only 10 nm below the metal interfaces. In addition to the 3.4 eV bandgap and associated phonon replica peaks, these spectra show sub-bandgap features due to native point defects. At room temperature, only a broad peak at ~ 2.5 eV appears for both metals, associated with oxygen vacancies $V_O$. [41] For Au, Fig. 4(a) left shows only gradual increases in this peak with annealing until 650 °C, at which temperature a second peak due to zinc vacancies $V_{Zn}$ appears at ~ 2 eV [42]. The appearance of $V_{Zn}$ corresponds to exceeding the phase diagram's eutectic temperature boundary for Au–Zn eutectic formation [43] and the resultant outdiffusion of Zn into the Au, leaving behind $V_{Zn}$ just below the interface. In contrast, the Fig. 4(b) Left Ta-ZnO(000–1) interface shows only the initial $V_O$ feature, which grows relative to the near band edge (NBE) features with increasing temperature.

These defect changes correlate with Schottky and ohmic I–V properties of their respective interfaces. For the left-side low defect DRCL spectra, I–V characteristics show that: (a) Au–ZnO Schottky contacts remain rectifying up to a 550 °C anneal and (b) the more reactive Ta contacts are initially ohmic, then blocking when annealed and stable up to 550 °C. This blocking corresponds to formation of an insulating $Ta_2O_5$ interface layer, whose bandgap emission DRCLS indeed detects [40]. For high defect ZnO with orders of magnitude higher defect intensity, the Au-ZnO(000–1) interface is now ohmic at all temperatures, due to defect-assisted tunneling through the Schottky barrier, whereas the Ta–ZnO(000–1) interface is initially ohmic, then blocking at 450 °C as the $Ta_2O_5$ forms, then less blocking as the higher density defect-assisted tunneling begins [40]. In general, these experimental results show that macroscopic electrical measurements correlate directly with nanoscale measurements of defects at intimate semiconductor interfaces. Furthermore, they establish that macroscopic Schottky barrier and ohmic behavior has a nanoscale physical basis.

Scanning electron microscopy (SEM) enables 3-dimensional DRCLS measurements of native point defects inside state-of-the-art device structures. Figure 5(a) shows an AlGaN/GaN high electron mobility transistor (HEMT) structure illustrating the ability of DRCLS to probe laterally between source and drain, laterally along the gate-drain interface, and in depth across and below the 2DEG AlGaN interface layer [44, 45]. Besides defect peak intensities, the semiconductor bandgap energy is sensitive to temperature T, decreasing with increasing T, and crystal lattice strain σ, increasing with increasing σ, so that these critical materials parameters can be measured in 3 dimensions while the device is operating. Three-dimensional DRCLS hyperspectral imaging (HSI) maps of T and σ at conventional power levels (not shown) [46, 47] show increases at the drain-side gate edge, consistent with finite difference simulations and Raman spectroscopy [48]. Figure 5(b) shows DRCLS defect measurements vs depth through the drain-side gate, revealing 2.8–3.0 eV blue band (BB) and 3.75 eV AlGaN deep-level defect densities localized in the $Al_xGa_{1-x}N$ strain layer [44]. The increase in defect density in this layer is consistent with the inverse piezoelectric effect, now believed responsible for $Al_xGa_{1-x}N$/GaN HEMT degradation due to current leakage through strain-induced defects [49, 50].

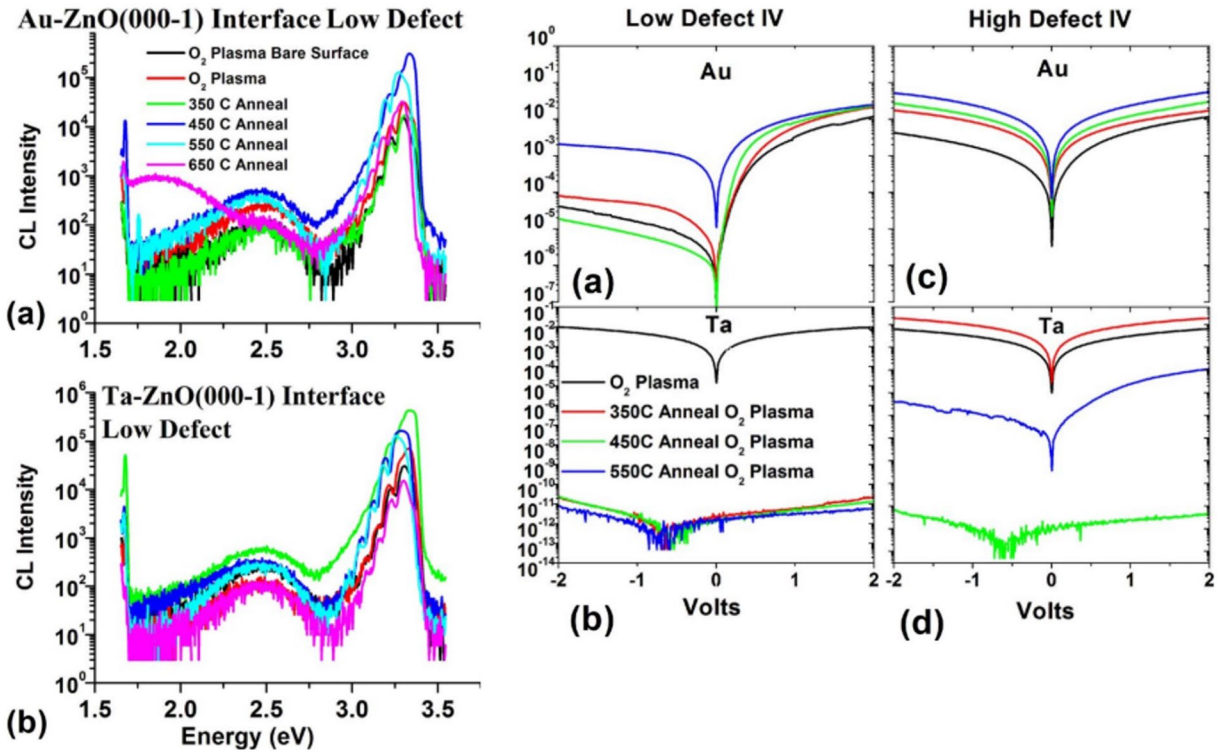


**Figure 4:** *Left*: 5 keV, 10 K DRCLS of 30 nm (a) Au and (b) Ta deposited on low defect (000–1)ZnO. For Au, annealing induces only slight changes for $T < 650$ °C but a large ~ 2 eV peak at 650 °C. Initial Ta deposition triples 2.5 eV emission, but annealing induces no ~ 2 eV emission or further 2.5 growth. *Right*: (a) Low defect Au contacts remain rectifying with annealing up to 550 °C whereas (b) high defect Au contacts are first ohmic then blocking with annealing. High defect *I-V* characteristics show (c) Au Schottky barrier steadily degrading starting at 350 °C and (d) Ta contacts that become blocking at 450 °C with leakage increasing at 550 °C. Both metals show lower thermal stability vs low defect ZnO [40].

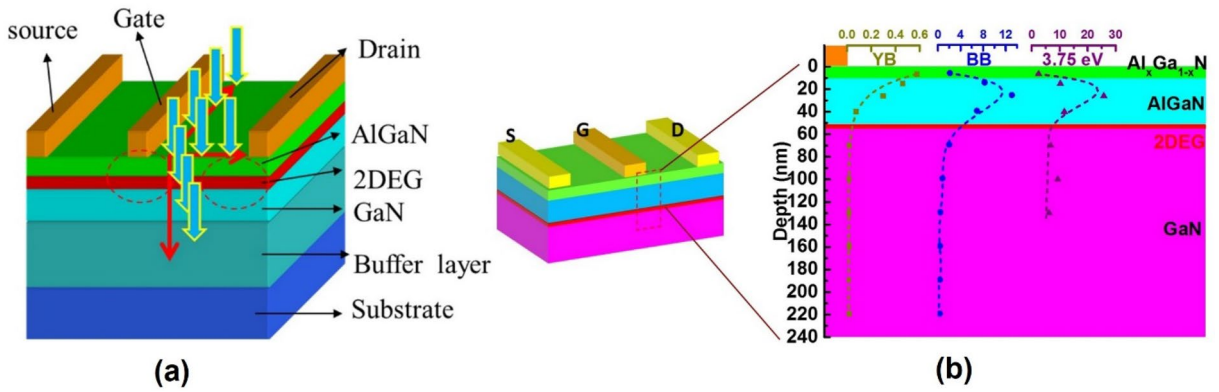


**Figure 5:** (a) DRCLS of AlGaN/GaN high electron mobility transistor (HEMT). Arrows signify probe location and depth of excitation. (b) AlGaN/GaN HEMT structure with dashed rectangle indicating region near the drain-side gate edge where yellow band (YB), blue band (BB), and 3.75-eV AlGaN deep-level defect densities are measured versus depth [44].

Defects in another state-of-the-art device structure involve an ultrawide bandgap semiconductor, $Ga_2O_3$, one of the latest advanced electronic materials and a prime candidate for high power applications due to its high dielectric breakdown strength. With a bandgap of 4.8 eV, $Ga_2O_3$ represents a challenge to optical excitation measurements of native point defects. However, with electron beam excitation to generate electron–hole pair creation of even such high or higher bandgap materials, together with nanometer-scale secondary electron microscopy (SEM), one can now study the defect distributions inside $Ga_2O_3$ devices and their movement under applied electric fields [51] Fig. 6(a) shows a characteristic CL

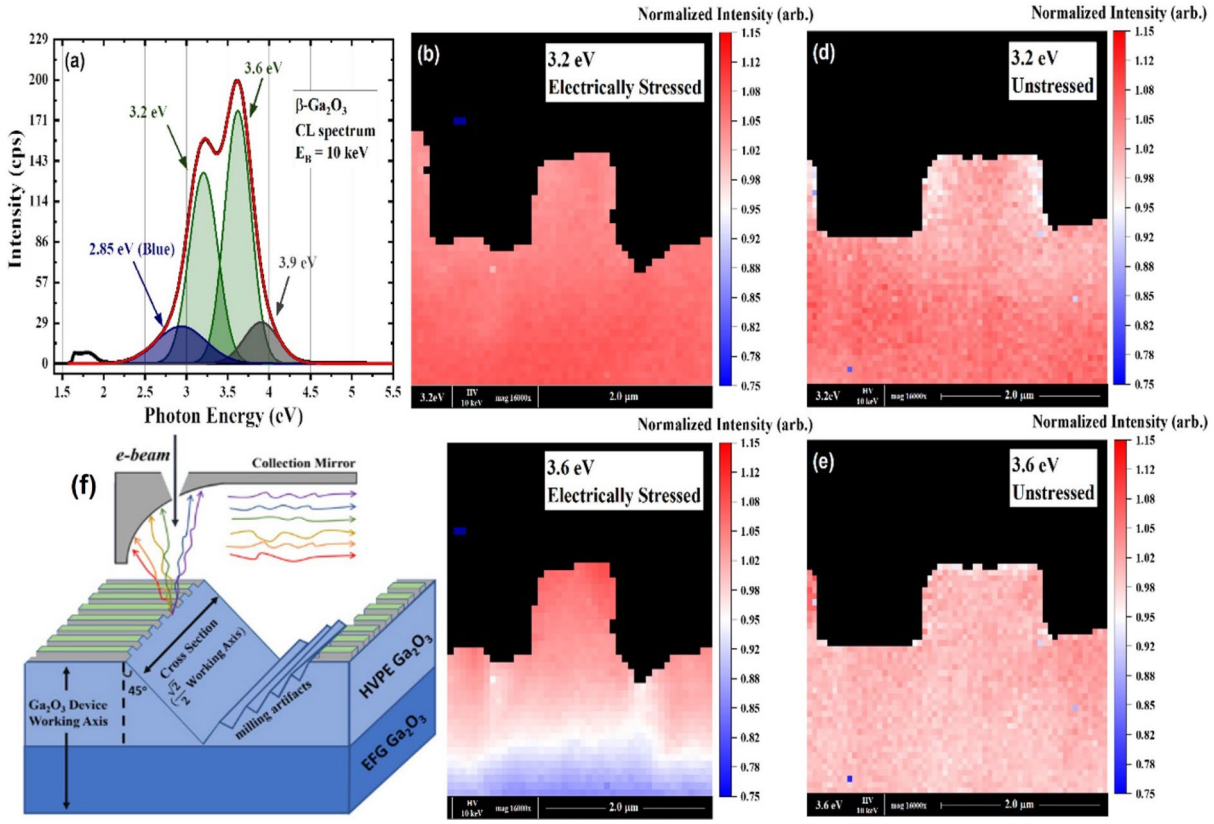


**Figure 6:** (a) Representative CL spectra of $Ga_2O_3$ vertical Schottky barrier diode (SBD) deconvolved with four Gaussian peaks at 2.85, 3.2, 3.6, and 3.9 eV. (b) and (c) Hyperspectral images (HSIs) of an electrically stressed $Ga_2O_3$ vertical device showing relative redistributions of 3.2 and 3.6 eV features. Highly segregated 3.6 vs 3.2 eV CL defect intensities are evident near the trench corners with pronounced gradients extending 1 μm below, while the fins exhibit only minor variation. (d) and (e) HSI of an unstressed device showing uniform peak distributions before electrical stress. (f) CL acquisition setup showing $Ga_2O_3$ vertical SBD angled cross section with parabolic collection mirror in position [51].

spectrum of β-phase $Ga_2O_3$ with dominant features at 3.2 and 3.6 eV attributed to Ga vacancies $V_{Ga}$ and O vacancies $V_O$, respectively. Since $V_{Ga}$ and $V_O$ act as acceptors and donors, respectively, in $Ga_2O_3$, they are electrically charged and subject to applied electric fields. Figures 6(b) and (c) display the HSI maps of these defects in an electrically stressed vertical trench Schottky diode in cross section involving quasi-static reverse current–voltage measurements from 0 V to breakdown ($V_{br}$ ≈—2 kV). Figure 6(b) shows an increase in 3.2 eV emission increasing away from the cathode fin structure compared with the unstressed cross section in Fig. 6(d). Conversely, Fig. 6(c) shows an increase toward the cathode fin structure compared with the unstressed cross section in Fig. 6(e). The increase in donor density, albeit a deep level unless complexed with H, can increase the effective electric field gradient around the fin structure. While other physical effects such as self-trapped excitons [52] and interstitial hydrogen [53] may also contribute to the CL features, these also involve native point defects [51]. The movement of semiconductor defects under applied electric fields adds another dimension to their importance in materials research.

## Combining optical, electronic, and microscopic techniques

Combining SEM-based DRCLS with scanning transmission electron microscopy (STEM), the materials science of the metal/$Ga_2O_3$ interface can now be probed at the nanometer to atomic scale *within the same near-interface volume*, revealing metal diffusion, lattice distortion, new defect and phase formation, and the opportunity to understand interface behavior under extreme electric fields leading to dielectric breakdown. This can become a new direction for the study of electronic material defects and their impact on next-generation electronics.

A recent study of defects at a metal–$Ga_2O_3$ interface provides an example of the information provided by the combination of DRCLS and STEM. Defects associated with Ir, a common impurity in edge-fed growth $Ga_2O_3$, can affect carrier transport and recombination, particularly at high device processing and operating temperature and at metal interfaces [54]. Figure 7 shows DRCL spectra taken through vs adjacent to Ir diodes on $Ga_2O_3$ as the insets illustrate.

In addition to the common 3.2 and 3.6 eV defects already shown in Figs. 6 and here in Fig. 7(b), the electron

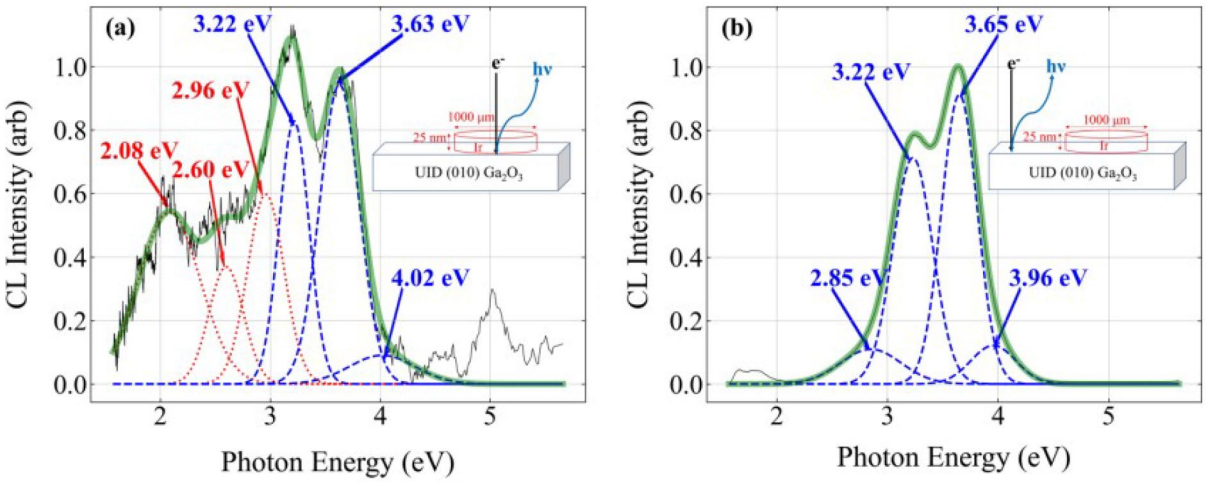


**Figure 7:** Representative as-deposited CL spectra for (a) the Ir– $Ga_2O_3$ interface at $E_B = 1.4$ keV, with Ir-related emissions (dotted lines) and (b) an adjacent bare $Ga_2O_3$ surface. Insets show the dimensions of the Schottky contacts and probe geometries on vs off the contacts. Deconvolved peak emissions due to $Ga_2O_3$ intrinsic vs Ir-induced defects are denoted by dashed vs dotted lines, respectively. The solid line envelope denotes the overall spectral fit [54].

beam-deposited Ir induces new $Ga_2O_3$ defect emissions in the 2–3 eV range, consistent with charge state transitions for Ir in $Ga_2O_3$ predicted by theory [55]. These defect features extend 10–20 nm past the interface, indicative of Ir diffusion into the $Ga_2O_3$. With rapid thermal annealing (RTP) in $N_2$, these defects extend tens of nm to almost 100 nm with a calculated diffusivity high enough to suggest that lattice inhomogeneities can provide enhanced diffusion pathways. The Ir diffusion can also account for dramatic changes in I–V, C–V, series resistance and ideality factor characteristics by increasing charge carrier recombination through these Ir-induced defects as well as dipole formation that can account for a + 1 V shift in I–V minimum [54].

A STEM map of a corresponding RTP Ir- $Ga_2O_3$ diode in Fig. 8 shows: (i) unusually high intensity at Ga columns, which indicates Ir substitutional atoms (blue arrow), (ii) the extra intensity in between the Ga columns, which indicates the interstitial Ir atoms (red arrow), and (iii) a group of bright atoms (cyan arrow) that indicate clustering of Ir atoms and potentially indicative of Ir-O structure. Using a quantitative atomic counting method [56], the number of Ir atoms in all three defect types

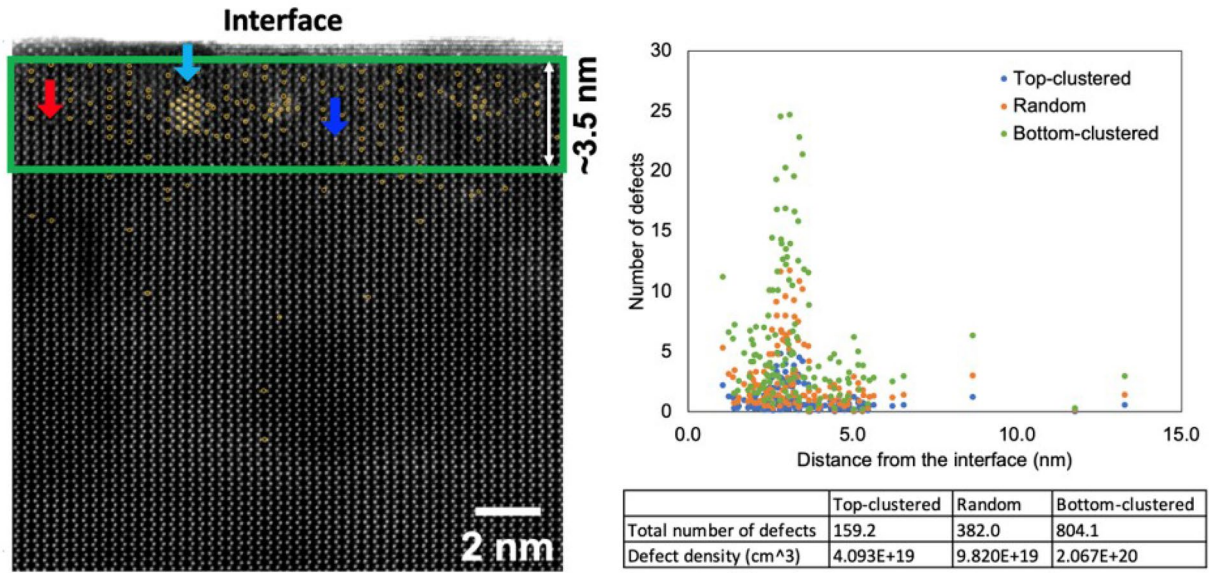


| | Top-clustered | Random | Bottom-clustered |
|---|---|---|---|
| Total number of defects | 159.2 | 382.0 | 804.1 |
| Defect density (cm^3) | 4.093E+19 | 9.820E+19 | 2.067E+20 |

**Figure 8:** (*Left*). Cross-sectional, high angular dark field STEM image of 700 °C annealed Ir-$Ga_2O_3$ interface showing Ir-related defects. (*Right*) Number of Ir atoms as a function distance from the interface including 3 types of Ir defects [54].

was counted vs distance from the interface. Within 5 nm of the interface, Ir defect densities ranged from between $4.1 \times 10^{19}$ $cm^{-3}$ and $2.1 \times 10^{20}$ $cm^{-3}$ with most of the Ir defects appearing within 3.5 nm. This demonstrated that the DRCLS-derived diffusion lengths are similar to those found by direct physical observation. Indeed, these densities provide an estimate of only 1–1.8 nm spatial separation for one of the dominant Ir-induced defects in Fig. 6(a), helping to illustrate the contribution of defect-assisted tunneling to a nearly 3-order of magnitude observed increase in reverse-bias current [54].

These combined DRCLS—STEM studies of the Ir- $Ga_2O_3$ interface also provide evidence for new phase formation as shown by the additional CL peaks at energies above the 4.8 eV β-$Ga_2O_3$ bandgap, consistent with the presence of higher bandgap polymorphs. Ongoing DRCLS-STEM studies of other annealed metal– $Ga_2O_3$ interfaces also exhibit CL features characteristic of lattice distortion [57], new defect [58], and new phase formation associated with metal indiffusion [59]. In addition, the locally high densities of defects created near semiconductor–metal interfaces at elevated temperatures may play a role in dielectric breakdown.

## New interface defect research: challenges and opportunities

The next research frontier for defects at electronic materials interface involves several significant challenges but corresponding opportunities as well. These challenges are both experimental and theoretical, while the corresponding opportunities are both fundamental and applied. Table 1 provides examples of both.

Describing materials properties at semiconductor–metal interfaces in 3 dimensions is a challenge requiring atomic scale chemical and structural measurements of bonding and composition changes. This is an opportunity for STEM, which can now measure (i) lattice structure phase changes in both interfacial layers and nanoscale inclusions [59]; (ii) composition from EDX or ELS core level absorption thresholds; and (iii) chemical bond changes from EDX or ELS.

Measuring semiconductor band structure at nanoscale distances from metal interfaces is challenging for optical techniques, which typically involve sub-micron or larger absorption depths. The opportunity is for techniques such as DRCLS, which can measure bandgap and sub-bandgap defect emissions locally in 3 dimensions. To determine band bending, XPS and UPS can measure Fermi-level movements in the semiconductor bandgap of clean semiconductor surfaces stepwise with atomic layer deposition of metals in UHV.

Correlating macroscopic barrier measurement to nanoscale electronic features is a challenge since macroscopic barrier height measurements are affected by defect charges and electric dipoles at the nanoscale. The opportunity is for STEM with EDX, which can measure new interface lattice phases, metal indiffusion, lattice distortion, atomic interstitials, and vacancies. DRCLS can measure new defect states near interfaces nondestructively and correlate them depth-wise to STEM features. The charge associated with these features can be related to electric dipole voltages measured macroscopically to account for Schottky barrier heights.

Controlling macroscopic barriers with nanoscale materials changes is a challenge requiring controlled material processes. The opportunity is for surface science and remote plasma chemistry combined with near-nm DRCLS to introduce controlled interface dipole changes, which can be monitored *in operando* for any changes as device structure are operated.

A major challenge for high power devices is understanding the physical mechanisms of dielectric breakdown under extreme applied voltages since these mechanisms must be identified at the atomic scale. This is an opportunity for DRCLS combined with STEM, which together can identify atomic lattice and electrical defect changes and possible percolation pathways with extreme electric fields extending up to and beyond breakdown.

This is an exciting time for solid-state electronic materials with advanced micro- and optoelectronic properties, but native point defects at their semiconductor–metal interface can limit their operation. These defects depend strongly on interface chemical structure, and techniques are now available

**TABLE 1:** Measuring and controlling defects at semiconductor–metal interfaces: challenges and opportunities.

| Challenges | Opportunities |
|---|---|
| Describe materials properties at semiconductor–metal interfaces in 3 dimensions | Relate lattice structure phase changes to local chemical composition and bonding |
| Measure semiconductor band structure at nanoscale distances from metal interfaces | Follow energy band transitions locally with incremental metal overlayers |
| Correlate macroscopic barrier measurements to nanoscale electronic features | Determine defect charge densities and spatial distribution effect on interface dipoles |
| Control macroscopic barriers with nanoscale materials changes | Develop semiconductor surface treatments to create specific dipole layers |
| Identify dielectric breakdown mechanisms | Measure atomic lattice and defect spatial redistributions stepwise up to breakdown |

to learn how their presence at nanoscale dimensions impacts electronic structure. Combining these optical, electronic, and microscopic techniques can provide new directions for defect research of metal–semiconductor interfaces at the nano/atomic scale. In turn, they can meet the experimental challenges and create the opportunities for new defect research of electronic material interfaces at a deeper level.

## Acknowledgments

The author gratefully acknowledges Drs. Charles.F. Brucker (Kodak), Chung-Han. Lin (Intel), H.Lee Mosbacker (Traycer Diagnostics), Micah.S. Haseman (Diamond Foundry), Daram.N. Ramdin (Ohio State University) and Profs. Giorgio Margaritondo (Ecole Polytechnique Fédérale de Lausanne), and Jinwoo Hwang (Ohio State University) for their contributions featured in this review.

## Author contributions

The author designed the research projects whose results are presented here, organized the results of these projects reported here, wrote this review manuscript, revised the manuscript, and acquired the funding required to support the research.

## Funding

The author gratefully acknowledges the support from NSF grant DMR-18-00130 (T. Paskova) and AFOSR Grant No. FA9550-18-1-0066 (A. Sayir).

## Data availability

The data that support the findings of this study are available from the corresponding author upon reasonable request.

## Declarations

**Conflict of interest** The authors have no conflict of interest to disclose.

## Open Access



## References

1. Thin Films- Interdiffusion and Reactions, ed. J.M. Poate, K.N. Tu, and J.W. Mayer (Wiley-Interscience, New York, 1978). ISBN 0–471–02238–1
2. J. Bardeen, Surface States and rectification at a metal semiconductor contact. Phys. Rev. **71**, 717 (1947). https://doi.org/10.1103/PhysRev.71.717
3. MRS Online Proceedings Library 2 (1) (1980). https://link.springer.com/journal/43582/volumes-and-issues/2-1
4. C.B. Duke, Twenty years of semiconductor surface and interface structure determination and prediction: the role of the annual conferences on the physics and chemistry of semiconductor interfaces. J. Vac. Sci. Technol. B **11**, 1336–1346 (1993). https://doi.org/10.1116/1.586938
5. E.H. Rhoderick, R.H. Williams, *Metal-Semiconductor Contacts*, 2nd edn. (Clarendon Press, Oxford, 1988)
6. L.J. Brillson, The structure and properties of metal-semiconductor interfaces (North-Holland, Amsterdam). Surf Sci. Rep. **2**, 123–326 (1982). https://doi.org/10.1016/0167-5729(82)90001-2
7. I. Lindau, P. Pianetta, S. Doniach, W.E. Spicer, X-ray photoemission spectroscopy. Nature **250**, 214 (1974). https://doi.org/10.1038/250214a0
8. J.R. Waldrop, R.W. Grant, Interface chemistry of metal-GaAs Schottky-barrier contacts. Appl. Phys. Lett. **34**, 630 (1979). https://doi.org/10.1063/1.90642
9. L.J. Brillson, G. Margaritondo, N.G. Stoffel, R.S. Bauer, R.Z. Bachrach, G. Hansson, Measurement and modulation of atomic interdiffusion at Au-GaAs (110) interfaces. J. Vac. Sci. Technol. **17**, 880 (1980). https://doi.org/10.1116/1.570609
10. L.J. Brillson, Transition in Schottky barrier formation with chemical reactivity. Phys. Rev. Lett. **40**, 260 (1978). https://doi.org/10.1103/PhysRevLett.40.260
11. L.J. Brillson, C.F. Brucker, A.D. Katnani, N.G. Stoffel, G. Margaritondo, Chemical basis for InP-metal Schottky barrier formation. Appl. Phys. Lett. **38**, 784 (1981). https://doi.org/10.1063/1.92162
12. L.J. Brillson, C.F. Brucker, A.D. Katnani, N.G. Stoffel, G. Margaritondo, Atomic and electrical structure of InP-metal interfaces: a prototypical III-V compound semiconductor. J. Vac. Sci. Technol. **19**, 661 (1981). https://doi.org/10.1116/1.571081
13. L.J. Brillson, Coupled interface plasmons of Al films on CdSe and CdS. Phys. Rev. Lett. **38**, 245 (1977). https://doi.org/10.1103/PhysRevLett.38.245
14. L.J. Brillson, G. Margaritondo, N.G. Stoffel, Atomic modulation of interdiffusion at Au–Al/GaAs interfaces. Phys. Rev. Lett. **44**, 667 (1980). https://doi.org/10.1103/PhysRevLett.44.667

15. L.J. Brillson, C.F. Brucker, A.D. Katnani, N.G. Stoffel, G. Margaritondo, Abruptness of semiconductor-metal interfaces. Phys. Rev. Lett. **46**, 838 (1981). https://doi.org/10.1103/PhysRevLett.46.838
16. L.J. Brillson, C.F. Brucker, A.D. Katnani, N.G. Stoffel, R. Daniels, G. Margaritondo, Fermi level pinning and chemical structure of InP-metal interfaces. J. Vac. Sci. Technol. **21**, 564 (1982). https://doi.org/10.1116/1.571764
17. E.R. Weber, H. Ennen, U. Kaufmann, J. Windscheif, T. Wosinski, Identification of $As_{Ga}$ antisites in plastically deformed GaAs". J. Appl. Phys. (1982). https://doi.org/10.1063/1.331577
18. S.G. Louie, M.L. Cohen, Self-consistent pseudopotential calculation for a metal-semiconductor interface. Phys. Rev. Lett. **35**, 866 (1975). https://doi.org/10.1103/PhysRevLett.35.866
19. S.G. Louie, M.L. Cohen, Electronic structure of a metal-semiconductor interface. Phys. Rev. B **13**, 2461 (1976). https://doi.org/10.1103/PhysRevB.13.2461
20. J. Tersoff, Schottky barrier heights and the continuum of gap states. Phys. Rev. Lett. **52**, 465 (1984). https://doi.org/10.1103/PhysRevLett.52.465
21. P.W. Peacock, J. Robertson, Band offsets and Schottky barrier heights of high dielectric constant oxides. J. Appl. Phys. **92**, 4712 (2002). https://doi.org/10.1063/1.1506388
22. Yacobi, B. G.; Holt, D. B. Cathodoluminescence Microscopy of Inorganic Solids. (New York: Plenum, 1990) 292 pp. ISBN: 0306433141.
23. L.J. Brillson, A.P. Young, G.H. Jessen, T.M. Levin, S.T. Bradley, S.H. Goss, J. Bae, Low energy electron-excited nano-luminescence spectroscopy of GaN surfaces and interfaces. Appl. Surf. Sci. **175–176**, 442–449 (2001). https://doi.org/10.1016/S0169-4332(01)00098-8
24. A. Raisanen, L.J. Brillson, R.S. Goldman, K.L. Kavanagh, H.H. Wieder, Optical detection of misfit dislocation-induced deep levels at InGaAs/GaAs heterojunctions. Appl. Phys. Lett. **64**, 3572 (1994). https://doi.org/10.1063/1.111201
25. E.J. Miller, D.M. Schaadt, C.W. McKinney, E.T. Yu, X. Sun, L.J. Brillson, P. Waltereit, C. Poblenz, J.S. Speck, Origin and Microscopic mechanism for suppression of leakage currents in Schottky contacts to GaN grown by molecular-beam epitaxy. J. Appl. Phys. **94**, 7611–7615 (2003). https://doi.org/10.1063/1.1627460
26. B.D. White, M. Bataiev, S.H. Goss, X. Hu, A. Karmarkar, D.M. Fleetwood, R.D. Schrimpf, S.T. Pantelides, W.J. Schaff, and L.J. Brillson, "Electrical, Spectral, and Chemical Properties of 1.8 MeV Proton Irradiated AlGaN/GaN HEMT Structures as a Function of Proton Fluence," IEEE Trans. Nuclear Sci., Proc. 40th Annual Int'l Nucl. Space Radiation Effects Conf. 50 (6) 1934–1941 (2003). DOI: https://doi.org/10.1109/TNS.2003.821827
27. L.J. Brillson, A.P.Young, J. Schafer, H. Niimi, and G. Lucovsky, "Ultrathin Silicon Oxide and Nitride – Silicon Interface States," in Ultrathin SiO2 and High – K Materials for ULSI Gate Dielectrics, ed. H.R.Huff, M.L.Green, T.Hattori, G. Lucovsky, and C.A.Richter, Proc. Materials Research Society (MRS Press, Warrendale, PA, 1999) 567, pp.549–558. https://doi.org/10.1557/PROC-567-549
28. P.E. Smith, S.H. Goss, M. Gao, M.K. Hudait, Y. Lin, S.A. Ringel, L.J. Brillson, Atomic diffusion and band lineups at $In_{0.53}Ga_{0.47}As$-on-InP heterointerfaces. J. Vac. Sci. Technol. **B23**, 1832–1837 (2005). https://doi.org/10.1116/1.1949218
29. D. Doutt, H.L. Mosbacker, G. Cantwell, J. Zhang, J.J. Song, L.J. Brillson, Impact of near-surface defects and morphology on ZnO luminescence. Appl. Phys. Lett. **94**, 042111 (2009). https://doi.org/10.1063/1.3077015
30. T.M. Levin, G.H. Jessen, F.A. Ponce, L.J. Brillson, Localized states at InGaN/GaN quantum well interfaces. Appl. Phys. Lett. **75**, 3835–3837 (1999). https://doi.org/10.1063/1.125472
31. R.S. Okojie, D. Lukco, L.J. Brillson, S. Tumakha, G. Jessen, M. Zhang, P. Pirouz, Direct observation of oxidation-induced 4H-SiC – 3C-SiC polytypic transformation. Appl. Phys. Lett. **79**, 3056–3058 (2001). https://doi.org/10.1063/1.1415347
32. L.J. Brillson, S. Tumakha, G.H. Jessen, R.S. Okojie, M. Zhang, P. Pirouz, Thermal and doping dependence of 4H-SiC polytype transformation. Appl. Phys. Lett. **81**, 2785–2787 (2002). https://doi.org/10.1063/1.1512816
33. M. Hetzer, Y.M. Strzhemechny, L.J. Brillson, M.A. Contreras, A. Zunger, Direct Observation of copper depletion and potential changes at copper indium gallium diselenide grain boundaries. Appl. Phys. Lett. **86**, 162105–162107 (2005). https://doi.org/10.1063/1.1906331g
34. J. Zhang, S. Walsh, C. Brooks, D.G. Schlom, L.J. Brillson, Depth-resolved cathodoluminescence spectroscopy study of defects in $SrTiO_3$. J. Vac. Sci. Technol. B **26**, 1466 (2008). https://doi.org/10.1116/1.2918315
35. M.M. Rutkowski, K. McNicholas, Z.Q. Zeng, F. Tuomisto, L.J. Brillson, Optical identification of oxygen vacancy formation at $SrTiO_3$-(Ba, Sr)$Ti_O$3 heterostructures. J. Phys. D Appl. Phys. **47**, 255303 (2014). https://doi.org/10.1088/0022-3727/47/25/255303Selectedbytheeditorsfor'Highlightsof2014collection'
36. L.J. Brillson, Applications of Depth-resolved cathodoluminescence spectroscopy. J. Phys. D Appl. Phys. **45**, 183001–183027 (2012). https://doi.org/10.1088/0022-3727/45/18/183001
37. L.J. Brillson, Surfaces and Interfaces of Electronic Materials (Wiley-VCH, Weinheim, 2010). Ch. 22. ISBN: 9783527409150
38. A. Rose, "The Acoustoelectric effects and the energy losses by hot electrons-part II. RCA Rev. **27**, 600–631 (1966)
39. D. Drouin, A.R. Couture, D. Joly, X. Tastet, V. Aimez, R. Gauvin, CASINO V2.42—A fast and easy-to-use modeling tool for scanning electron microscopy and microanalysis users. Scanning **29**, 92 (2007). https://doi.org/10.1002/sca.20000
40. H.L. Mosbacker, C. Zgrabik, A. Swain, S. El Hage, M. Hetzer, D.C. Look, G. Cantwell, J. Zhang, J.J. Song, L.J. Brillson, Thermally driven defect formation and blocking layers at

metal-ZnO interfaces. Appl. Phys. Lett. **91**, 072102 (2007). https://doi.org/10.1063/1.2772664
41. F. Leiter, H. Alves, D. Pfisterer, N.G. Romanov, D.M. Hofmann, B.K. Meyer, Oxygen vacancies in ZnO. Phys. B **340–342**, 201–204 (2003). https://doi.org/10.1016/j.physb.2003.09.031
42. Y. Dong, F. Tuomisto, B.G. Svensson, AYu. Kuznetsov, L.J. Brillson, Vacancy defect and defect cluster energetics in ion-implanted ZnO. Phys. Rev. B. **81**, 081201(R) (2010). https://doi.org/10.1103/PhysRevB.81.081201
43. E. A. Brandes , *Smithells Metals Reference Book*, 6th ed. (Butterworth, London, 1983),Chap.11, p. 94. ISBN-13 978–0750636247
44. L.J. Brillson, G.M. Foster, J. Cox, W.T. Ruane, A.B. Jarjour, H. Gao, H. von Wenckstern, M. Grundmann, I. Hyland, M.W. Allen, Defect characterization, Imaging, and control in wide band gap semiconductors and devices. J. Electron. Mat. **47**, 4980–4986 (2018). https://doi.org/10.1007/s11664-018-6214-9
45. Chung-Han. Lin, Tyler A. Merz, D.R. Doutt, Jungwoo Joh, Jesus A. Del, U.K. Mishra. Alamo, Leonard J. Brillson, Strain and temperature dependence of defect formation at AlGaN/GaN high electron mobility transistors on a nanometer scale. IEEE Trans. Electron. Dev. **59**, 2667–2674 (2012). https://doi.org/10.1109/TED.2012.2206595
46. C.-H. Lin, T.A. Merz, D.R. Doutt, M.J. Hetzer, J. Joh, J.A. del Alamo, U.K. Mishra, L.J. Brillson, Nanoscale mapping of temperature and defect evolution inside operating AlGaN/GaN high electron mobility transistors. Appl. Phys. Lett. **95**, 033510 (2009). https://doi.org/10.1063/1.3189102
47. C.-H. Lin, D.R. Doutt, U.K. Mishra, T.A. Merz, L.J. Brillson, Field-induced strain degradation of AlGaN/GaN HEMTs on a nanometer scale. Appl. Phys. Lett. **97**, 223502 (2010). https://doi.org/10.1063/1.3521392
48. J.W. Pomeroy, M. Kuball, D.J. Wallis, A.M. Keir, K.P. Hilton, R.S. Balmer, M.J. Uren, T. Martin, P.J. Heard, Thermal mapping of defects in AlGaN/GaN heterostructure field-effect transistors using micro-Raman spectroscopy. Appl. Phys. Lett. **87**, 103508 (2005). https://doi.org/10.1063/1.2041823
49. J.A. del Alamo, J. Joh, GaN HEMT reliability. Microelectron. Reliab. **49**(9–11), 1200–1206 (2009). https://doi.org/10.1016/j.microrel.2009.07.003
50. J. Joh, F. Gao, T. Palacios, J.A. del Alamo, A model for the critical voltage for electrical degradation of GaN high electron mobility transistors. Microelectron. Reliab. **50**(6), 767–773 (2010). https://doi.org/10.1016/j.microrel.2010.02.015
51. Micah S. Haseman, Daram N. Ramdin, Wenshen Li, Kazuki Nomoto, Debdeep Jena, Huili Grace Xing, Leonard J. Brillson, Electric field induced migration of native point defects in $Ga_2O_3$ devices. J. Appl. Phys. **133**, 035701 (2023). https://doi.org/10.1063/5.0124543
52. J.B. Varley, A. Janotti, C. Franchini, C.G. Van de Walle, Role of self-trapping in luminescence and p-type conductivity of wide-band-gap oxides. Phys. Rev. B **85**, 081109(R) (2012). https://doi.org/10.1103/PhysRevB.85.081109
53. Mu. Sai, M. Wang, J.B. Varley, J.L. Lyons, D. Wickramaratne, C.G. Van de Walle, Role of carbon and hydrogen in limiting n-type doping of monoclinic $(Al_xGa_{1-x})_2O_3$. Phys. Rev. B **105**, 155201 (2022). https://doi.org/10.1103/PhysRevB.105.155201
54. D.N. Ramdin, M.S. Haseman, H.-L. Huang, K.D. Leedy, J. Hwang, L.J. Brillson, Optical and electronic effects of rapid thermal annealing at Ir-$Ga_2O_3$ interfaces. J. Appl. Phys. **131**, 205302 (2022). https://doi.org/10.1063/5.0090161
55. J.R. Ritter, J. Huso, P.T. Dickens, J.B. Varley, K.G. Lynn, M.D. McCluskey, Compensation and hydrogen passivation of magnesium acceptors in β-$Ga_2O_3$. Appl. Phys. Lett. **113**, 052101 (2018). https://doi.org/10.1063/1.5044627
56. J.M. Johnson, H.-L. Huang, M. Wang, S. Mu, J.B. Varley, A.F.M.A. Uddin Bhuiyan, Z. Feng, N.K. Kalarickal, S. Rajan, H. Zhao, C.G. Van de Walle, J. Hwang, APL Mater. **9**, 051103 (2021). https://doi.org/10.1063/5.0039769
57. J.M. Johnson, Z. Chen, J.B. Varley, C.M. Jackson, E. Farzana, Z. Zhang, A.R. Arehart, H.-L. Huang, A. Genc, S.A. Ringel, C.G. Van de Walle, D.A. Muller, J. Hwang, Unusual formation of point defect complexes in the ultra-wide band gap semiconductor β-Ga2O3. Phys. Rev. X **9**, 041027 (2019). https://doi.org/10.1103/PhysRevX.9.041027
58. Hsien-Lien. Huang, Jared M. Johnson, Christopher Chae, Alexander Senckowski, Man Hoi Wong, Jinwoo Hwang, Atomic scale mechanism of β to γ phase transformation in gallium oxide. Appl. Phys. Lett. **122**, 251602 (2023). https://doi.org/10.1063/5.0156009
59. D.N. Ramdin, M. S. Haseman, H.-L. Huang, K. D. Leedy, J. Hwang, and L. J. Brillson, unpublished